PLASMA SURFACE FUNCTIONALIZATION OF AFP MANUFACTURED COMPOSITES FOR IMPROVED ADHESIVE BOND PERFORMANCE

Ibrahim Sarikaya[1], Malik Tahiyat[1], Ramy Harik[1], Tanvir Farouk[1], John Connell[2], and Peter Gilday[1]

[1] McNAIR Center for Aerospace Innovation and Research, Department of Mechanical Engineering, College of Engineering and Computing, University of South Carolina
1000 Catawba St., Columbia, SC, 29201, USA

[2] NASA Langley Research Center,
Hampton, VA, 23681, USA

ABSTRACT

Application of carbon fiber reinforced polymer (CFRP) as a high-performance structural material has widespread application in the present aerospace industry. However, as-processed composite materials require a comprehensive surface treatment prior to bonding to remove contaminants and impart surface functionality and topography to overcome their poor adhesion properties. Atmospheric pressure plasma jet treatment (APPJT) has been increasingly garnering attention as an alternate method for surface preparation of CFRP. This method has been reported to achieve success in imparting favorable polar functional groups into the composite surfaces enhancing wettability and surface energy of the bonded surfaces. In some cases, APPJT has been demonstrated to remove contaminants or, in the case of silicones, convert them to silica. In this study, an atmospheric pressure plasma jet (APPJ) system was used for surface activation of a composite laid-up by an automated fiber placement (AFP) machine. Surface modifications prior to and after treatment were characterized using water contact angle (WCA) measurements, X-ray photoelectron spectroscopy (XPS), scanning electron microscopy (SEM), and atomic force microscopy (AFM). Double cantilever beam (DCB) tests were performed to quantify the bonding performance of the composites. The results show a marked enhancement of the mode I interlaminar fracture toughness with the application of APPJT.

1. INTRODUCTION

In the aerospace industry, adhesive bonds are commonly incorporated in CFRP structures due to several favorable factors: convenience, low-cost, low-stress concentration zones and uniform load transferring capability [1]. Thus, it has the potential to address several disadvantages associated with conventional mechanical fasteners like increased weight, high fabrication cost, and high stress zones [2-4]. However, due to the uncertainty associated with adhesive bonds, secondary arrest features are required for certification of bonded assemblies in safety critical applications. A strong, reliable adhesive bond is not achievable between CFRPs without a comprehensive surface preparation since as-processed CFRPs typically have surface contamination such as mold release that contributes to poor adhesion properties, low surface energy, poor wettability and consequently low interlaminar shear strength [5]. Surface preparation plays a vital role in improving interaction

SAMPE Conference Proceedings. Charlotte, NC, May 20-23, 2019. Society for the Advancement of Material and Process Engineering – North America.

between adhesive and composite surfaces by removing residual contaminants, creating active polar sites on the surface and increasing surface roughness [5, 6]. These, in turn, enhance wettability [7], and hence, surface energy [6], thus improving bond quality.

Non-thermal or low-temperature plasma treatment like APPJ treatment has garnered interest in recent years due to its ability to treat complex surfaces, being a non-contacting process and requiring minimal operator involvement [8]. APPJT has been shown to be versatile in incorporating favorable topographical modifications without influencing bulk properties [3, 5], resulting in an increase in surface roughness and potential removal of surface contaminants [9]. It excels in creating a high volume of hydrophilic surfaces [8] through surface functionalization [3, 10-12] without expensive vacuum equipment [9, 13]. APPJT has the added benefits of being a nonaqueous method and not producing any environmentally detrimental byproducts [9, 11, 14, 15].

In this study, the effects of APPJT on AFP manufactured CFRP were investigated with varying treatment speeds. Variations in surface wettability and adhesion were analyzed with contact angle measurements and XPS was used to quantify surface chemical modifications. SEM and AFM were used to investigate surface morphological and topographical changes. Lastly, DCB test was performed to assess bonding effectiveness through measuring mode I interlaminar fracture toughness with and without APPJT. Lastly, failure modes were analyzed by visual inspection and classified in accordance with ASTM D5573-99 [16].

2. EXPERIMENTATION

2.1 Composite fabrication and test coupon preparation

A CFRP panel was manufactured with Hexcel® IM7/8552 prepreg, with dimensions of 63.5 cm x 91.5 cm (25” x 36”) and a thickness of 0.127 cm (0.05”). The panel was fabricated in a unidirectional configuration $[0]_9$ by an IMT-LYNX® AFP machine and cured in a Bondtech® autoclave for 2 hours at a temperature of 177 °C (350 °F).

Laminates 15.25 cm x 23 cm (6” x 9”) were cut from this panel with a waterjet to prepare panels for subsequent treatment and adhesive bonding. The laminates were classified as: P (pristine), HW (pristine samples wiped with isopropyl alcohol wipes) and treated (HW samples that undergo APPJT). A single DCB assembly is formed from either bonding two HW or two treated laminates.

Two laminates were bonded, one atop the other with Metlbond® 1515-3M film adhesive. A fluorinated ethylene propylene (FEP) polymer film was used at the top of the laminate assembly to serve as a crack starter for the DCB test configuration. The bonded laminates were cured in a Bondtech® autoclave under vacuum at 660 Torr (26” Hg) at a pressure of 0.31 MPa (45 psi). The temperature inside the autoclave was increased to 177 °C (350 °F) at 2.8 °C/min (5 °F/min), held at 177 °C (350 °F) for 2 hours, and then decreased to 49 °C (120 °F) at 2.8 °C/min (5 °F/min). The laminates were then cut into 2.54 cm x 17.8 cm (1” x 7”)individual specimens, and finally, two aluminum piano hinges were bonded with J-B Weld adhesive to each of these segments to form a coupon. Each coupon was then cured for 24 hours at room temperature.

2.2 Characterization

The surface chemical composition up to a depth of 10 nm of the composite was investigated with a Kratos® Axis Ultra XPS system. A Surface Analyst device SA3001 (Brighton Technologies Group, Inc., Cincinnati, OH) was used to measure contact angles on pristine, HW and treated surfaces. A Tescan® Vega3 SEM was used to study the surface morphology with a magnification of 1000x and 5000x. The surface topography was also studied at room temperature and under ambient conditions using an atomic force microscope (AFM) with Nanoscope® Dimension 3100 Controller. Scanning was achieved in a 5 µm by 5 µm area in non-contact mode with a NCH-10 silicon tip which has a radius of curvature of 2-5 nm, resonance frequency of 320 kHz, and a nominal spring constant of 42 N/m.

2.3 Atmospheric pressure plasma jet treatment

The plasma treatment was accomplished with an RD1004 plasma nozzle and FG5002 generator by Plasmatreat® (Steinhagen, Germany) operating at atmospheric pressure together with an XY translational stage as shown in Figure 1. The following process parameters were used: (1) treatment speed(s) of 0.254 cm/s [0.1 in/s (S1)] and 2.54 cm/s [1.0 in/s (S2)], (2) treatment overlap of 50 % and (3) working distance of 0.63 cm (0.25") from plasma jet to the composite surface.

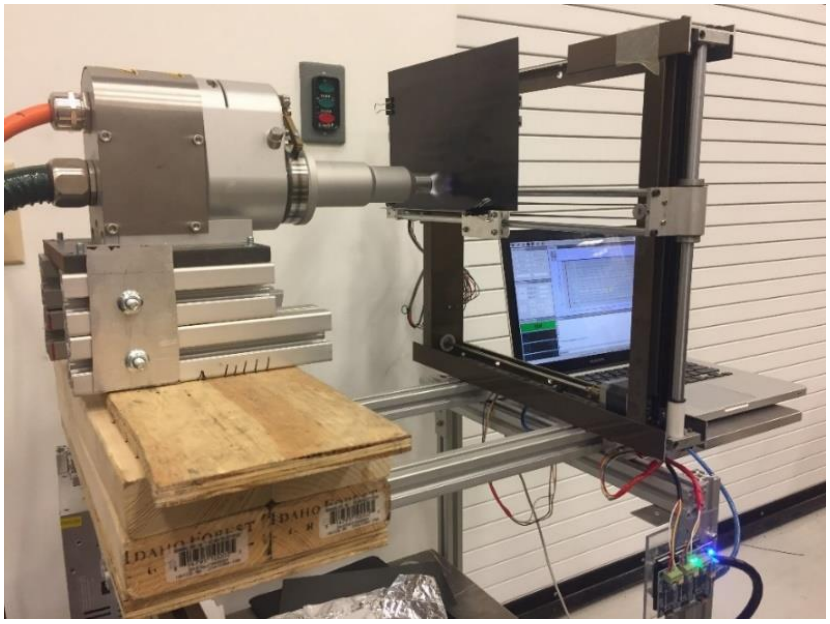

Figure 1 Atmospheric pressure plasma jet treatment system

2.4 Double Cantilever Beam Test

The DCB test was performed as shown in Figure 2 according to ASTM D5528 [17]. The loading rate of the tensile clamps was set at 2.54 cm/ min (1.0 in/min). The crack propagation along test coupon as well as the load-displacement data were simultaneously recorded with digital cameras in order to correlate the load and the delamination length.

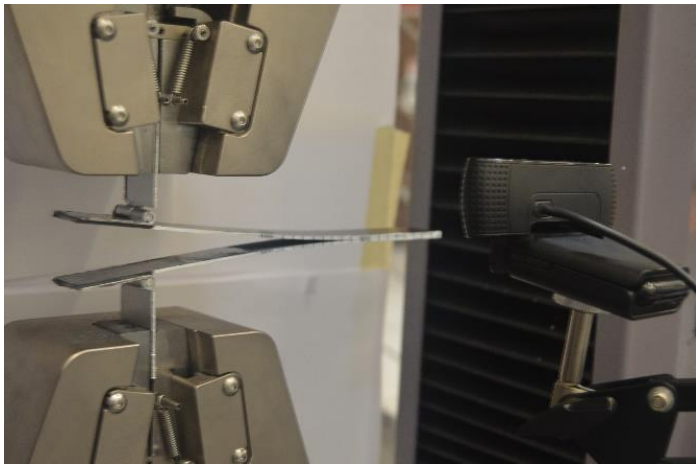

Figure 2 DCB test

Mode I interlaminar fracture toughness (G_{IC}) was calculated with Equation 1 according to the modified beam theory [17].

$$G_{IC} = \frac{3P\delta}{2b(a + |\Delta|)} \quad (1)$$

where G_{IC} is Mode I interlaminar fracture toughness, P is the load, δ is load point deflection, b is the width, a is the delamination length, $|\Delta|$ is effective delamination extension to correct for rotation of DCB arms at delamination front.

Interlaminar fracture toughness (G_{IP}) was also calculated with Equation 2:

$$G_{IP} = \frac{A}{ba} \quad (2)$$

where G_{IP} is fracture toughness calculated according to the area method, and A is the area under the load-displacement curve.

3. RESULTS

3.1 Surface Modification

XPS survey spectral analysis of the CFRP samples before and after APPJT are shown with oxygen to carbon atomic ratio (O/C) in
Table **1**. The HW samples were found to contain ~2-3.5% silicon by atomic concentration. The inclusion of this contaminant can be explained by the usage of a mold release agent during the manufacturing process (Frekote 710-NC), which consists of silicone compounds and polymers. XPS survey scan analysis shows that oxygen content increased by almost 100% after HW samples undergo APPJT. Oxygen to carbon atomic ratio (O/C) which represents the level of functionalization [18] increased significantly after treatment for both the treatment speeds. It is also seen that % increase in O/C with S1 was higher than that with S2. This is expected since a slower treatment speed would produce a more oxygenated surface due to longer treatment duration.

Table 1 XPS elemental analysis for pristine and treated composite samples

Specimen	Chemical composition (%)					Atomic ratio (%)	% increment	
	C	O	N	S	Si	O/C	O	O/C
HW1	72.17	18.25	4.58	1.60	3.39	25	100	248
T.S1	42.11	36.68	10.20	6.60	2.56	87		
HW2	76.50	15.24	4.89	1.19	2.15	20	99	160
T.S2	57.91	30.33	6.99	2.47	2.39	52		

Fractional composition of functional groups was deduced from high-resolution spectra of C 1s, O 1s and Si 2p and the results are tabulated in Table 2. Only the deconvolution of high-resolution C 1s spectra is shown in Figure 3 as an example. The C 1s peak for HW has been deconvoluted into four components at approximately 284.6, 285.9, 288.5 and 289.6 eV, which were assigned to 'C=C', 'C-N/C-C/C-O', 'O-C=O', and 'C-O' bonds respectively [19]. Both Table 2 and Figure 3 show a massive decrease in the functional group of 'C=C', and an increase in the functional groups of 'O-C=O' and 'C-O' in C 1s spectra and 'C=O' in O 1s spectra after APPT. A similar trend is observed in case of Si 2p spectra in which, there was a sharp fall in 'SiC', accompanied by a rise in 'SiO_2' at binding energies of 103.3 and 105 eV [20, 21] respectively after treatment. This indicates that the silicone species (which are known to be detrimental to adhesive bonding) from the mold release agent are converted to silica species which do not appear to have an effect on adhesion. An increase in surface oxygen content should result in an increase in surface energy, improved wettability, and potentially adhesive bond strength [12].

Table 2 XPS contributions of functional groups (%)

Chemical bond/group	C 1s				O 1s		Si 2p		
	C=C	C-N/C-C/C-O	O-C=O	C-O	C-O	C=O	SiO_2		SiC
Binding energy (eV)	284.6	285.9 ±0.2	288.5 ±0.2	289.6 ±0.2	532 ±0.2	533.3 ±0.2	103.3 ±0.2	105	101.8 ±0.1
HW1	65.4	30.2	4.4	-	80.9	19.1	27	-	73
T.S1	33.7	37.2	17	12.1	76.1	23.5	66.2	33.8	-
HW2	70	24.1	5.9	-	79.6	20.4	30.7	-	69.3
T.S2	45.6	39.1	15.3	-	60	40	75.4	-	24.6

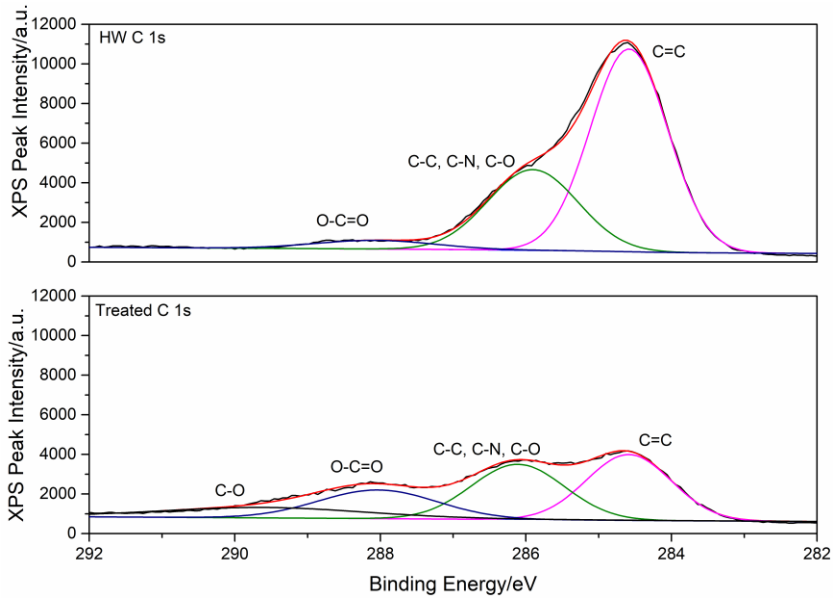

Figure 3 Sample 1 Carbon deconvolution analysis

Comparison of water contact angle measurements among pristine, HW and treated samples is shown in Figure 4. It is observed that the contact angle progressively decreased from pristine to HW to APPJ treated. A decrease in WCA is associated with higher surface hydrophilicity and higher polar groups on the surface [11]. An anomalous phenomenon to be noted is that a higher contact angle resulted from the lower treatment speed (S1). This is contrary to what was expected since a slower treatment was hypothesized to produce greater hydrophilicity compared to the faster treatment speed. This phenomenon might be attributed to the prolonged treatment time required at S1, which may have caused activated sites at the initiation of the treatment cycle to deactivate by reaction with atmospheric radicals, hence increasing WCA.

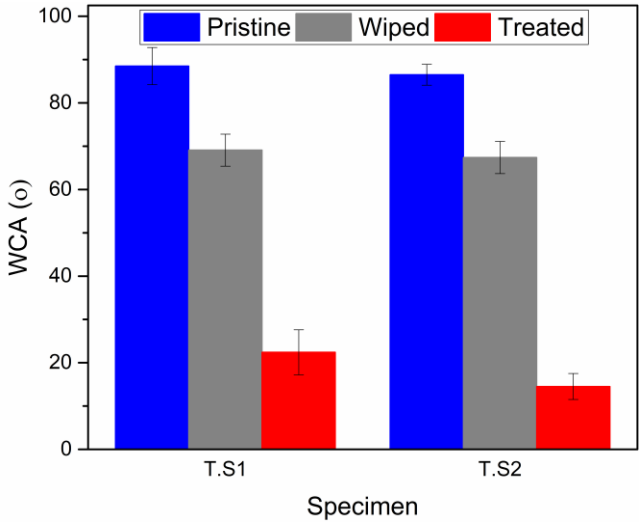

Figure 4 WCA for pristine, wiped and treated laminates

SEM images of sample 1 and sample 2 are shown with magnifications 1000x and 5000x for HW and treated samples in Figure 5 and Figure 6 Sample 2 SEM images: at 1000x a) HW b) T.S2; at 5000x c) HW d) T.S2, respectively. It can be seen that pristine samples had a relatively smooth surface with

a very faint outline of fibers in both the HW (Figure 6 Sample 2 SEM images: at 1000x a) HW b) T.S2; at 5000x c) HW d) T.S2a) and the specimen treated at S2 (Figure 6 Sample 2 SEM images: at 1000x a) HW b) T.S2; at 5000x c) HW d) T.S2c). For longer treatment duration, as shown in Figure 5(b & d), the fibers in the same region gained a more prominent outline, which suggests some surface ablation might have occurred. White areas on Figure 5d may indicate oxidation sites since these appear at the lower treatment speed only. SEM results, however, do not show any noticeable damage to the fibers after treatment.

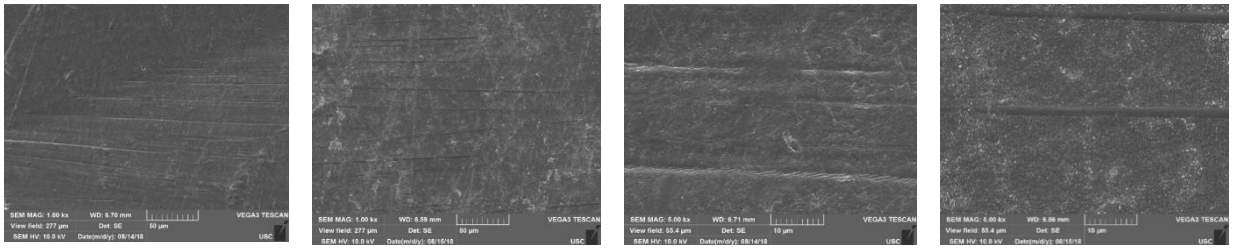

(a) (b) (c) (d)

Figure 5 Sample 1 SEM images: at 1000x a) HW b) T.S1; at 5000x c) HW d) T.S1

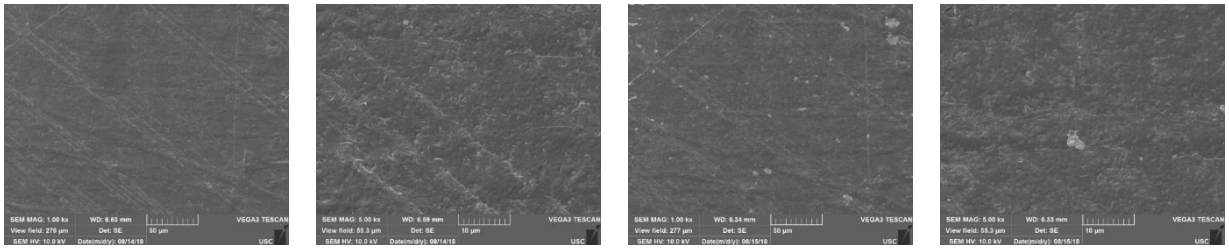

(a) (b) (c) (d)

Figure 6 Sample 2 SEM images: at 1000x a) HW b) T.S2; at 5000x c) HW d) T.S2

The surface topographical changes prior to and after plasma treatment are shown in Figure 7 and Figure 8 and the results tabulated in Table **3**. It is seen that for S1, several prominent peak-valley distributions resulted from APPJT as shown in Figure 7b. This corresponded to an increase in roughness by ~10 nm. For the higher treatment speed (S3), the peak-valley distribution was more succinct with roughness increasing by ~6.5 nm after treatment. Thus, APPJT indeed imparts roughness on a nanometer scale. Higher surface roughness for sample 1 can be attributed to the higher treatment duration. Even though higher surface roughness is associated with higher adhesion property [9], in our experimentation, the increase in roughness from the APPJT is too small between the samples to say conclusively if the increase in roughness would play a significant role in enhancing adhesive properties.

Table 3 Mean surface roughness

Specimens	Roughness (nm)	Roughness (nm)
HW	25.307	16.954
Treated	35.170 (T.S1)	23.647 (T.S2)

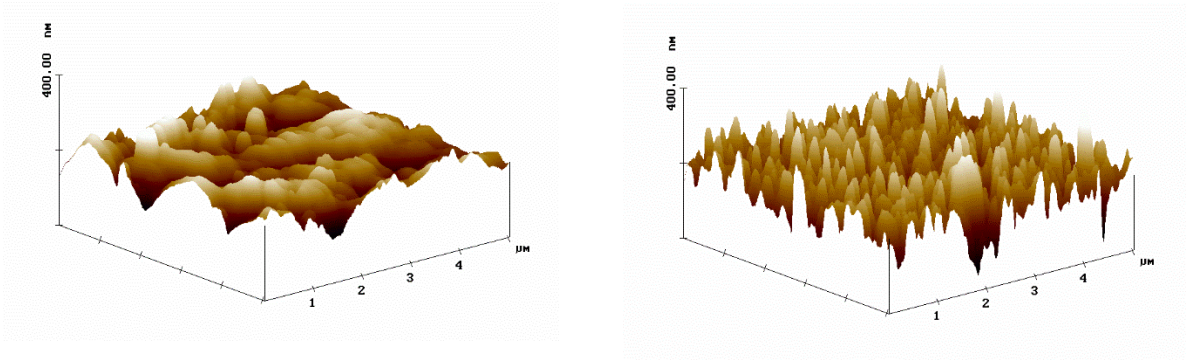

(a) (b)

Figure 7 Sample 1 3D images a) HW b) Treated (T.S1)

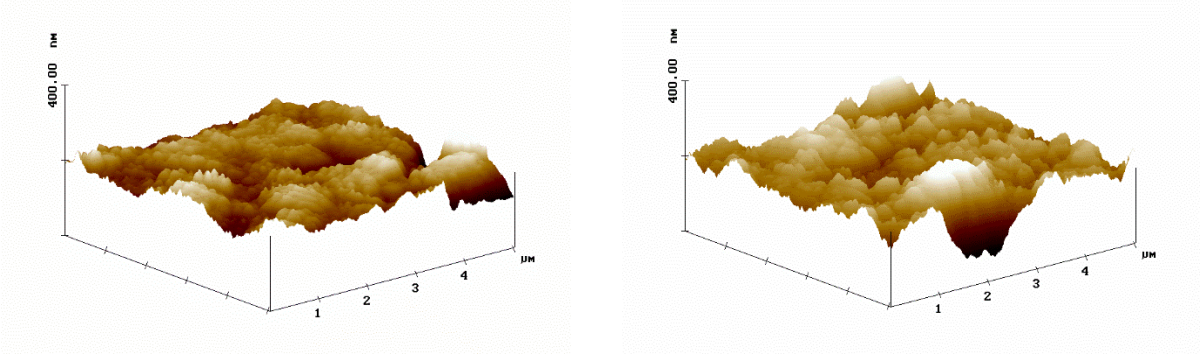

(a) (b)

Figure 8 Sample 2 3D images a) Pristine b) Treated (T.S2)

3.2 Double Cantilever Beam Test

Load-displacement plots of three coupon assemblies (HW, T.S1, and T.S2) in **Error! Reference source not found.** show that coupons made from laminates with APPJT can sustain much higher failure loads than those made from HW laminates. Additionally, **Error! Reference source not found.** shows that the fracture toughness of T coupons, irrespective of treatment speed, is found to be at least twofold higher than that of HW coupons. Failure interface of HW coupons showed that all of those underwent adhesive failure whereas every T coupon failed cohesively, hence, depicting stronger adhesive bonding for T coupons. This is likely due to the ineffectiveness in the HW process to remove silicone contaminants, create surface functionality, or increase roughness (see XPS data). Thus, it can be stated that APPJT increases the fracture toughness of coupons compared to only using alcohol wipes. Average fracture toughness (G_{IP}) in Figure 10 and the mode I delamination resistance curve (R curve) as a function of delamination growth in Figure 11 correlate well with each considering that both show a noticeable increase in fracture toughness and resistance to delamination for treated coupons, especially for the sample treated at a slower treatment speed.

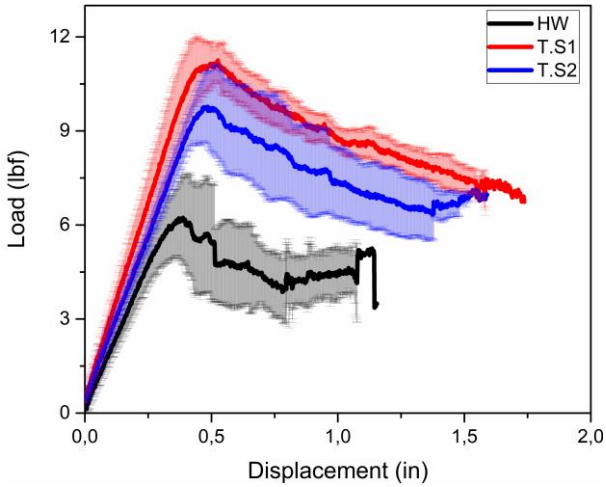

Figure 9 Load-displacement curves of HW, T.S1 and T.S2

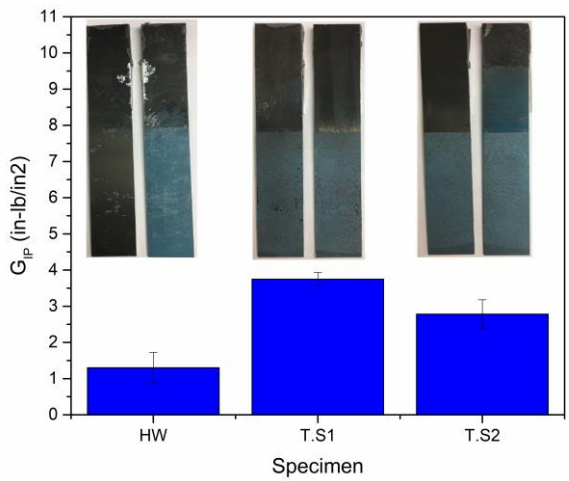

Figure 10 G_{IP} results and failure modes of DCB tests for HW, T.S1 and T.S2

This difference can be explained with enhanced O/C ratio and higher polar functional groups which increased adhesion [3, 8, 22]. Results represent that the hydrophilic behavior of sample 1 with lower treatment speed S1 was higher according to G_{IC} and G_{IP}.

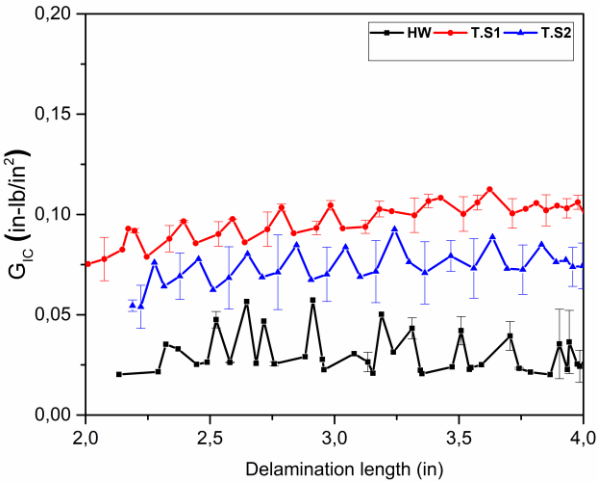

Figure 11 Mode I delamination resistance curve (R curve)

4. CONCLUSIONS

In this study, the effects of APPJT on CFRP surface properties have been studied on unidirectional CFRP laminates with two varying treatment speeds. XPS spectra showed a large proportion of the single and double bonded carbon groups undergoing oxidation after APPJT with the highest oxidation achieved at the slower treatment speed. This increase in oxygen-containing polar functional groups after plasma treatment resulted in a reduction in WCA and thus an increase in wettability and surface energy. SEM showed treated surfaces did not show any noticeable damage, but minor material removal might have been associated with the lower treatment speed. AFM showed that a higher rms roughness on the nanometer scale resulted from a lower treatment speed. Enhancement in surface activation, wettability, hydrophilicity, and roughness indicated from XPS,

WCA, SEM and AFM was reflected in the DCB results showing higher fracture toughness (G_{IP}) and a higher resistance to delamination (G_{IC}) after APPJ treatment, especially at a slower treatment speed.

5. ACKNOWLEDGEMENT

The authors would like to thank NASA Langley Research Center and the Advanced Composite Consortium. This research was funded by NASA under Award Nos. NNL09AA00A and 80LARC17C0004. The authors would like to thank the 2C26 CRT partners: Eileen Kutscha and Kay Blohowiak from the Boeing Company; Xiaomei Feng, Gurbinder Sarao, and Wenping Zhao from UTC Aerospace. The authors would like to also thank for their support in this project from BTG Labs: Gilles Dillingham, and Derrick Merrell; and Plasmatreat: Josh Schlup; Solvay: Alejandro Rodriguez. The authors are extremely grateful to Prof. Michael Sutton, Prof. Travis W Knight, Mechanical Engineering, and Dr. Stavros Karakalos, XPS facility, University of South Carolina for valuable consultation and resources. The authors would like to thank Cody Shuman, Megan Ryan, and Michael Haddad, undergraduate research assistants and McNAIR Junior Fellows at the University of South Carolina, for their research support.

Any opinions, findings, and conclusions or recommendations expressed in this material are those of the author(s) and do not necessarily reflect the views of the National Aeronautics and Space Administration.

6. REFERENCES

1. Pribanic, T., et al. *Effect of surface contamination on composite bond integrity and durability*. in *Proceedings of the 2012 Joint Advanced Materials Structures Center of Excellence 8th Annual Technical Meeting, Baltimore, MD*. 2012.
2. Oberhammer, J., F. Niklaus, and G. Stemme, *Selective wafer-level adhesive bonding with benzocyclobutene for fabrication of cavities.* Sensors and Actuators A: Physical, 2003. **105**(3): p. 297-304.
3. Encinas, N., et al., *Surface modification of aircraft used composites for adhesive bonding.* International Journal of Adhesion and Adhesives, 2014. **50**: p. 157-163.
4. Harik, R., et al. *Automated fiber placement defect identity cards: cause, anticipation, existence, significance, and progression*. in *Submission to SAMPE 2018 Conference & Exhibition, Long Beach, California, US*. 2018.
5. Tiwari, S. and J. Bijwe, *Surface treatment of carbon fibers-a review*. Procedia Technology, 2014. **14**: p. 505-512.
6. Luo, Y., et al., *Surface and wettability property analysis of CCF300 carbon fibers with different sizing or without sizing.* Materials & Design, 2011. **32**(2): p. 941-946.
7. Banea, M. and L.F. da Silva, *Adhesively bonded joints in composite materials: an overview.* Proceedings of the Institution of Mechanical Engineers, Part L: Journal of Materials: Design and Applications, 2009. **223**(1): p. 1-18.
8. Zaldivar, R., et al., *The effect of atmospheric plasma treatment on the chemistry, morphology and resultant bonding behavior of a pan-based carbon fiber-reinforced epoxy composite.* Journal of composite materials, 2010. **44**(2): p. 137-156.

9. Van Deynse, A., R. Morent, and N. De Geyter, *Surface modification of polymers using atmospheric pressure cold plasma technology.* Polymer Science: Research Advances, Practical Applications and Educational Aspects; Méndez-Vilas, A., Solano, A., Eds, 2016: p. 506-516.
10. Kusano, Y., T.L. Andersen, and P. Michelsen. *Atmospheric pressure plasma surface modification of carbon fibres*. in *Journal of Physics: Conference Series*. 2008. IOP Publishing.
11. Borcia, G., C. Anderson, and N. Brown, *The surface oxidation of selected polymers using an atmospheric pressure air dielectric barrier discharge. Part I.* Applied surface science, 2004. **221**(1-4): p. 203-214.
12. Li, H., et al., *Air dielectric barrier discharges plasma surface treatment of three-dimensional braided carbon fiber reinforced epoxy composites.* Surface and Coatings Technology, 2009. **203**(10-11): p. 1317-1321.
13. Encinas, N., et al., *Atmospheric pressure plasma hydrophilic modification of a silicone surface.* The Journal of Adhesion, 2012. **88**(4-6): p. 321-336.
14. Jones, C., *The chemistry of carbon fibre surfaces and its effect on interfacial phenomena in fibre/epoxy composites.* Composites science and technology, 1991. **42**(1-3): p. 275-298.
15. Morent, R., et al., *Non-thermal plasma treatment of textiles.* Surface and coatings technology, 2008. **202**(14): p. 3427-3449.
16. Standard, A., *D5573-99*. 1999, D5573-ADJ.
17. Astm, D., *5528-01*. Standard test method for mode I interlaminar fracture toughness of unidirectional fiber-reinforced polymer matrix composites, 2001.
18. Jordá-Vilaplana, A., et al., *Improvement of mechanical properties of polylactic acid adhesion joints with bio-based adhesives by using air atmospheric plasma treatment.* Journal of Applied Polymer Science, 2015. **132**(32).
19. Dementjev, A., et al., *X-Ray photoelectron spectroscopy reference data for identification of the C3N4 phase in carbon–nitrogen films.* Diamond and Related Materials, 2000. **9**(11): p. 1904-1907.
20. Webb, L.J., et al., *High-resolution X-ray photoelectron spectroscopic studies of alkylated silicon (111) surfaces.* The Journal of Physical Chemistry B, 2005. **109**(9): p. 3930-3937.
21. Birer, Ö., et al., *XPS investigation of thin SiOx and SiOxNy overlayers.* Journal of molecular structure, 1999. **480**: p. 611-614.
22. Encinas, N., J. Abenojar, and M. Martínez, *Development of improved polypropylene adhesive bonding by abrasion and atmospheric plasma surface modifications.* International Journal of Adhesion and Adhesives, 2012. **33**: p. 1-6.